Inverse demigration for simultaneous source separation

Chris Leader and Biondo Biondi

ABSTRACT

Separating simultaneously acquired seismic data is the link between more efficient acquisition and conventional imaging techniques. Existing methods for separation rely on coherency measurements and work only for randomly delayed sources. By using the extended image space, data blended with a variety of time delay sequences can be well separated. Demigration will then output the separated, conventionally equivalent, dataset. A single pass of demigration can adequately recreate kinematic information. For amplitude balancing, however, an inverse process is required. By introducing a blending operator into a linearised inverse system posed in the extended image space, accurate data separation is observed for a variety of blending schemes, without the need for an accurate velocity model. Furthermore, such a system can be easily adapted to include velocity model updates, since extended imaging has already been applied.

INTRODUCTION

Contemporary seismic targets are increasingly associated with steeply dipping structures and strong velocity contrasts. In order to illuminate these difficult features, data are acquired with large offsets and multiple source boats (Verwest and Lin, 2007). Intuitively, this leads to both more expensive acquisition and an increase in field waiting time. This latter adverse consequence is due to the fact that it is necessary to allow the energy from the previous source to sufficiently dissipate before recording the next source point. If waiting time was not a restriction then denser sampling could be recorded per unit time and acquisition would be significantly more efficient (Beasley (2008); Hampson et al. (2008); Berkhout and Blacquiere (2008)). Practically, it is possible to disregard this waiting time and fire the next shot when in position; this is often called continuous recording. Recording overlapping data in this manner requires more processing time than conventionally acquired data, since separation is necessary to mitigate imaging artifacts. However, the economic gains from reduced acquisition time far outweigh this extra processing cost.

These simultaneously acquired data can be used to directly invert for model properties (Dai and Schuster (2009); Tang and Biondi (2009)). However, such methods require exact knowledge of the velocity model. Separation and subsequent imaging is a viable option, since this could be integrated into production data flows. Successful

existing methods rely on random sampling in the source timings and locations (Abma and Yan (2009); Moore et al. (2008)). For example, constant receiver gathers can be transformed into the f-k or tau-p domain and iteratively thresholded (Doulgeris et al., 2011), removed in the parabolic random domain (Ayeni et al., 2011), removed by using a convex projection approach (Abma et al., 2010), or through compressive sensing methods (Herrmann et al., 2009).

Image domain processing has been used effectively for coherent energy removal / attenutation by posing the problem in the extended image space (Zhang and Duan (2013); Sava and Guitton (2005)). It is possible to untangle certain events in this domain and recreate cleaner shot gathers by virtue of higher signal-to-noise ratio and reduced dimensionality. Additionally, when using the extended image space (Sava and Vasconcelos, 2011), event kinematics are preserved. Consequently, if the velocity model is inaccurate then demigration is still possible (Chauris and Benjemaa, 2010).

In the previous SEP report (Leader and Biondi, 2014), methods of distinguishing events in the angle domain were analysed, with the goal of using curvature-based penalties during demigration. Whilst this method worked very well for simple scattering models, for highly heterogeneous structures the ranges of curvature necessary for demigration were too high. Additionally, describing the curvature using a single parameter became less possible. In this study a mass inverse demigration scheme will be postulated. By introducing a blending operator and posing the problem as a linearised inversion, accurate separation (in terms of both amplitudes and kinematics) is observed after a small number of iterations.

A range of model complexities and velocity inaccuracies will be analysed to test the strength of this methodology. Additionally, three blending strategies will also be tested - constant time delays, pseudo-constant time delays and purely random time delays.

DEMIGRATION

To accurately recreate all wavefield complexities, Reverse Time Migration (RTM) (Baysal et al., 1983) is the choice of imaging operator. RTM uses solutions to the full two-way wave equation (within physical assumptions), making it a valuable option for highly heterogeneous Earth models. Furthermore, RTM is the adjoint of Born modeling, and it is possible to move between the data and image spaces by combining these operators. For zero-offset imaging, these are summarised in equation 1 and equation 2. Examples of a Born modelled shot gather and an RTM image are shown in Figure 1 and Figure 2 respectively.

$$m(\mathbf{x}) = \sum_{\mathbf{x}_s,\omega} f(\omega) G_0(\mathbf{x}, \mathbf{x}_s, \omega) \sum_{\mathbf{x}_r} G_0(\mathbf{x}, \mathbf{x}_r, \omega) d^*(\mathbf{x}_r, \mathbf{x}_s, \omega), \tag{1}$$

$$d(\mathbf{x}_r, \mathbf{x}_s, \omega) = \omega^2 \sum_{\mathbf{x}} f(\omega) G_0(\mathbf{x}, \mathbf{x}_s, \omega) m(\mathbf{x}) \sum_{\mathbf{x}} G_0(\mathbf{x}, \mathbf{x}_r, \omega). \tag{2}$$

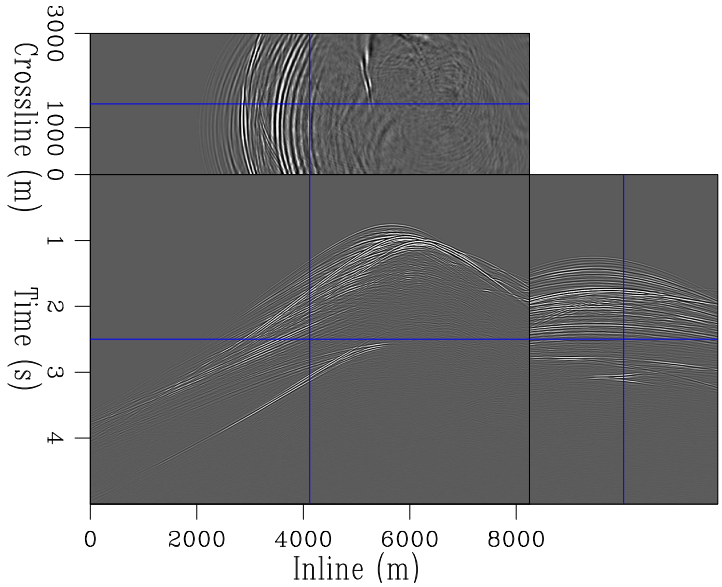

Figure 1: An example of a 3D shot gather produced from Born modeling. [**NR**]

here $\mathbf{x}$ represents the spatial coordinates, $m(\mathbf{x})$ the scattering field, $\mathbf{x}_s$ the current source coordinates, $\mathbf{x}_r$ the current receiver coordinates, ω the temporal frequency, $d^*(\mathbf{x}_r, \mathbf{x}_s, \omega)$ the complex conjugate of the data and G_0 the relevant Green's function. The aforementioned zero-offset image (Claerbout, 1971) is calculated here. For an accurate velocity model this will contain all necessary amplitude and kinematic information for demigration and hence data recovery.

However, for the problem of separating continuously acquired data a stringent requirement on the velocity model is undesirable. Direct application of equation 1 with an incorrect velocity model will result in the loss of certain events, and subsequent demigration will not represent the original dataset well. To preserve all event kinematics, extended imaging must be used. If zero-offset imaging can be described by equation 3, then extended imaging can be described by equation 4.

$$I(x, y, z) = \sum_{i}^{nshots} \sum_{t} P_s(x, y, z, t; \mathbf{s}_i) P_r(x, y, z, t; \mathbf{s}_i), \tag{3}$$

$$I(x, y, z, x_h, y_h) = \sum_{i}^{nshots} \sum_{t} P_s(x + x_h, y + y_h, z, t; \mathbf{s}_i) * P_r(x - x_h, y - y_h, z, t; \mathbf{s}_i). \tag{4}$$

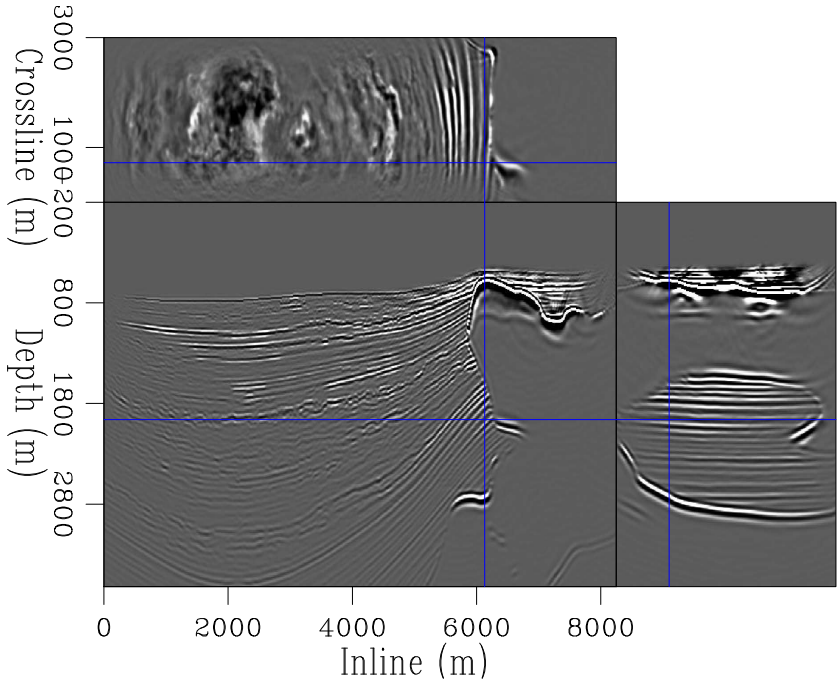

Figure 2: An example image produced from RTM over the SEAM velocity model, in 3D. [**NR**]

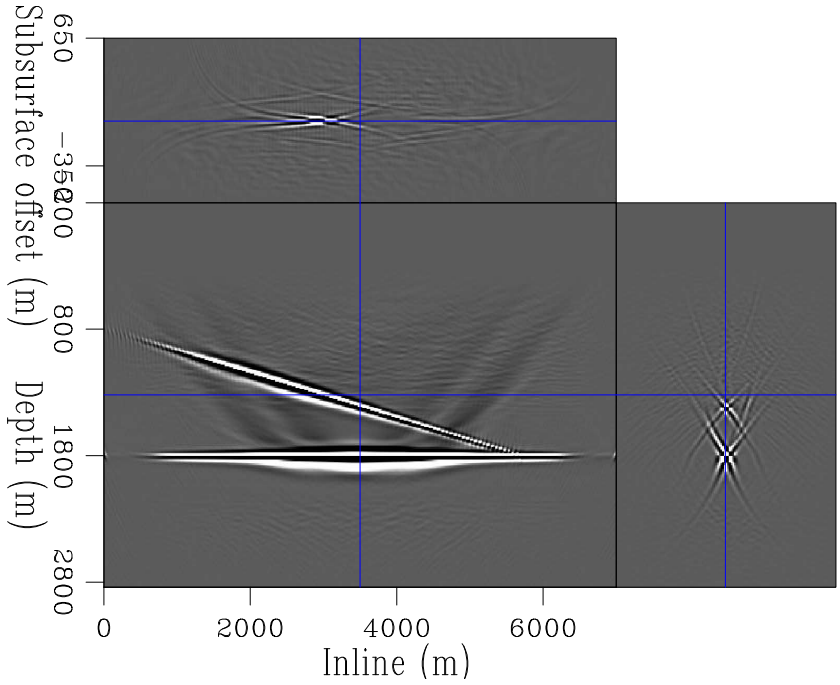

Figure 3: An extended image produced using an accurate velocity model. [**CR**]

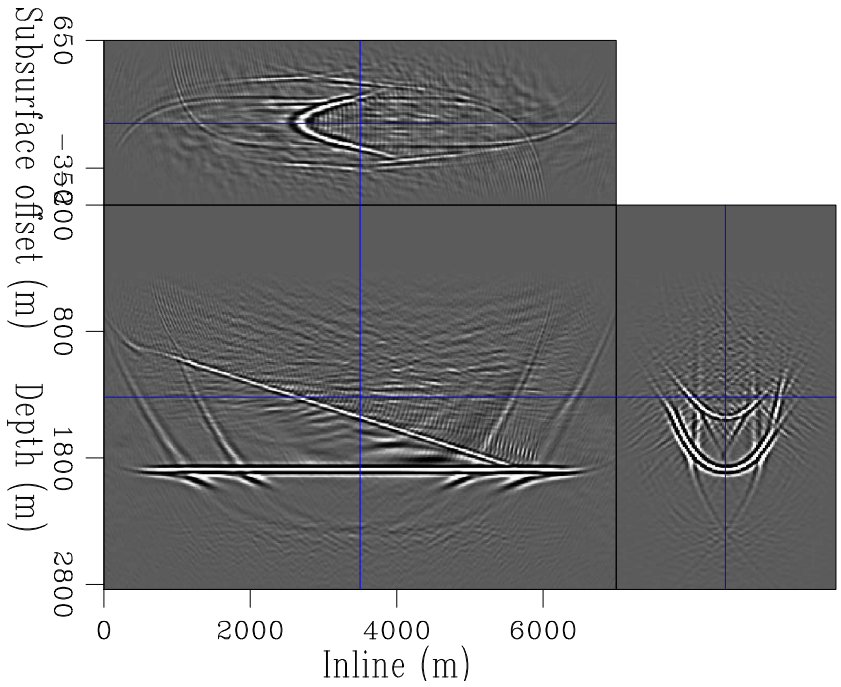

Figure 4: An extended image produced using an inaccurate velocity model. [**CR**]

Here, $I(x, y, z)$ is the image in space, P_s is the source wavefield and P_r is the receiver wavefield; s_i represents the current shot of interest. If lag coordinates (known as subsurface offsets) in x and y are introduced (x_h and y_h), a 5D image can be created. It is possible to have lags in both t and z to create a 7D image, or any combination thereof. From hereon this discussion will be limited to subsurface offsets in the x direction only.

If the correct velocity model were used for imaging then the energy will be focused to a point in subsurface offset, as seen in Figure 3. If an incorrect model were used then the energy will be spread out over a range of offsets (Figure 4). Analysing this moveout as a function of the velocity model is the core concept of Wave Equation Migration Velocity Analysis (WEMVA) (Sava et al., 2003).

To create Figure 2, equation 3 was used, and for Figure 3, equation 4 was used. By taking the adjoint of these processes and creating an extended Born modeling operator, demigration can be performed. The result from demigrating Figure 3 from the extended image domain to the data space is shown in Figure 5. Similarly, the result from demigrating Figure 4 is shown in Figure 6.

It is apparent that both passes of demigration have successfully recreated many of the data nuances - event kinematics are correctly positioned and all identifiable events in the input data are present in the demigrated data. However, frequency content has not been well preserved and event amplitudes at early times and short offsets are under represented. These imperfections are more pronounced when using the incorrect velocity model. Additionally, this result is more artifact laden. This is

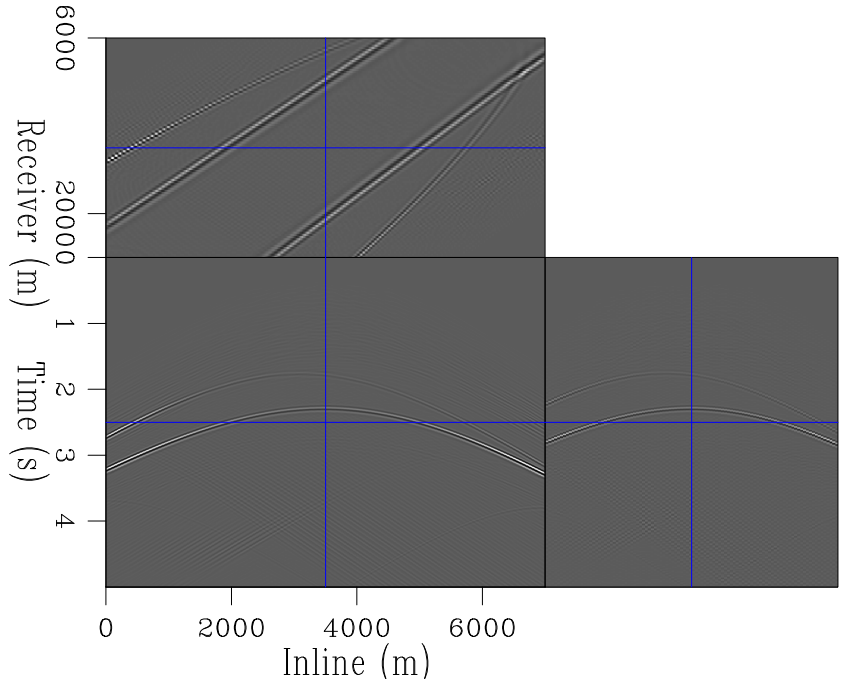

Figure 5: Adjoint demigration using the correct velocity model, in both directions. [**CR**]

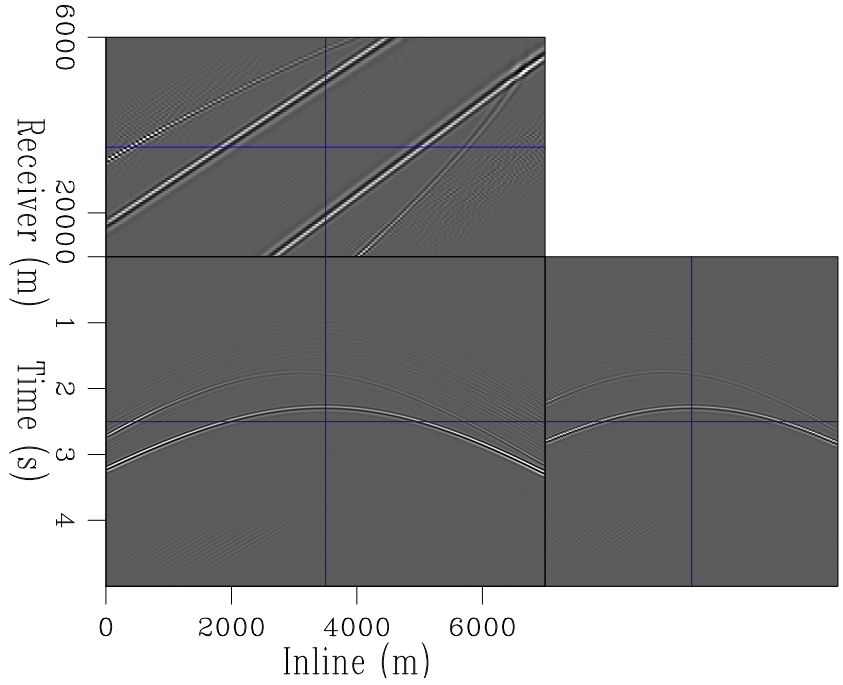

Figure 6: Adjoint demigration using an incorrect velocity model, in both directions. [**CR**]

a consequence of performing extended Born modeling, where the image convolution is shifted over a range of offsets.

INVERSE DEMIGRATION

To recover the correct amplitudes, adapting demigration to become an inverse process is necessary. In conventional Least-Squares RTM (LSRTM), RTM is used as the adjoint procedure, and Born modeling as the forward operator. A solver, such as conjugate directions, can then be used for model and residual updates. For inverse demigration almost exactly the same procedure can be used, but with the forward and adjoint operators swapped. The input will now be the extended image and the procedure will aim to recover the dataset that best represents the given image.

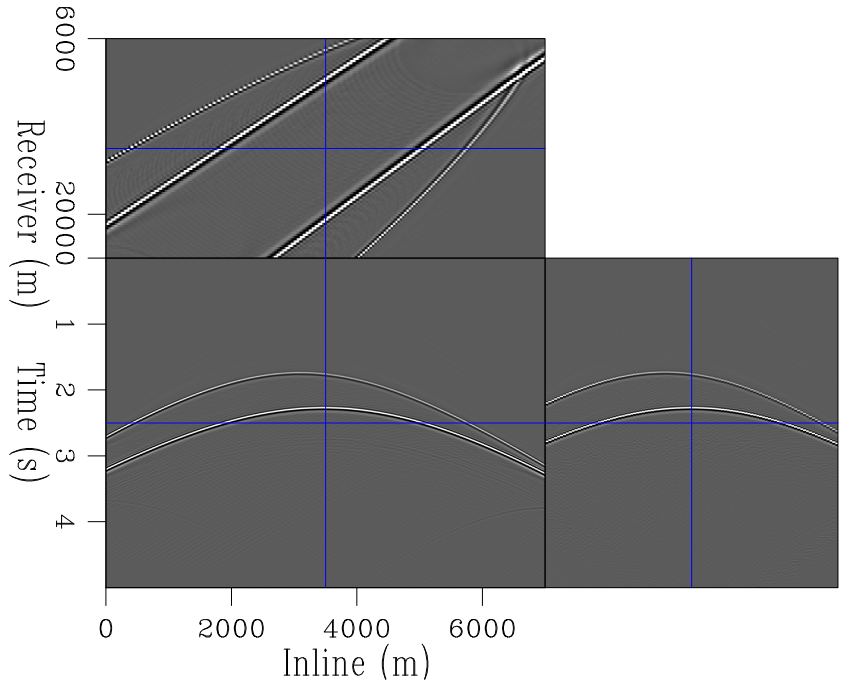

Figure 7: Inverse demigration, after ten iterations, using the correct velocity model. [**CR**]

Figure 7 and Figure 8 show the same recovered data as Figure 5 and Figure 6 respectively, after ten iterations of inverse demigration. Amplitudes are now consistently balanced and match the input data Furthermore, the vast majority of the artifacts from the incorrect velocity result are mitigated. The data-space residual, as a function of iteration number, can be seen in Figure 9.

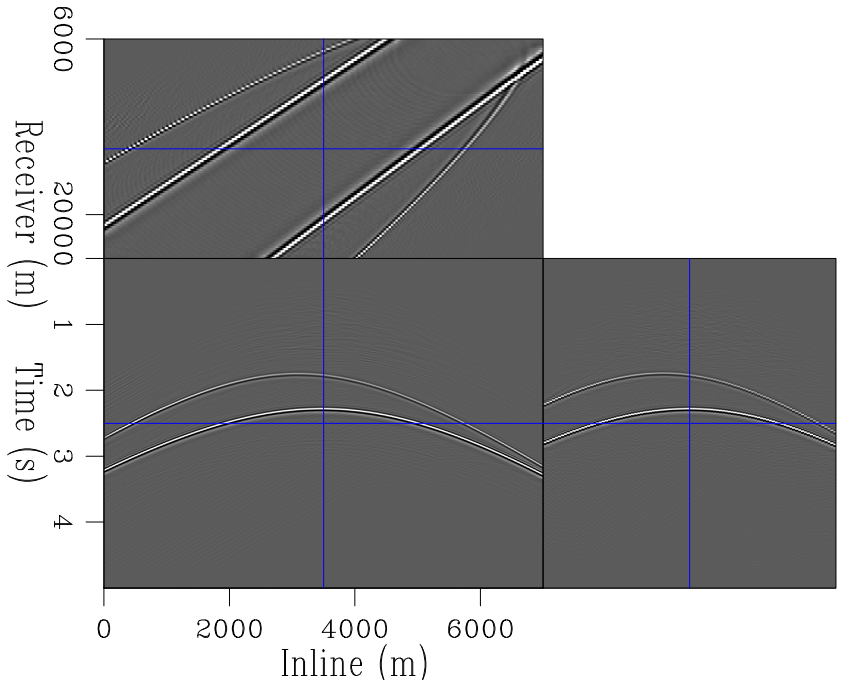

Figure 8: Inverse demigration, after ten iterations, using an incorrect velocity model. [**CR**]

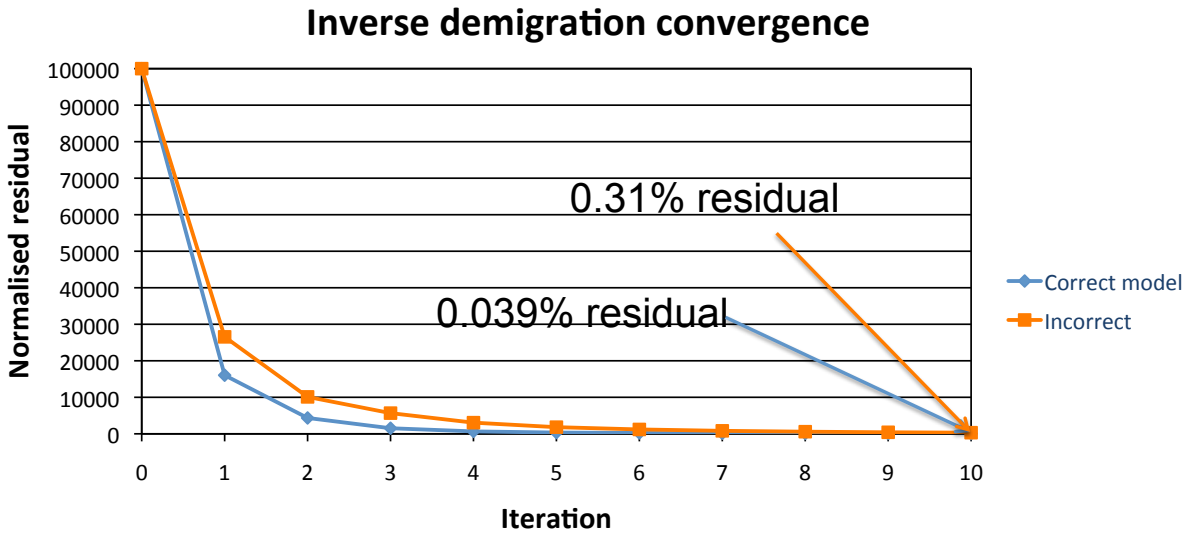

Figure 9: Data-space residual as a function of iteration number, for both correct and incorrect velocity model inverse demigration. [**NR**]

SIMULTANEOUS SHOT SEPARATION

Now that inverse demigration has been demonstrated to accurately recover input reflection data, the system can be adapted to provide shot separation. The input data will be the overlapping, simultaneously recorded dataset, so an additional operator must be included to account for the blending. This operator, Γ, will be referred to as the 'blending' operator, for obvious reasons. The forward process of Γ will take a conventional dataset, then delay and sum the shots together to produce a continuous record. The adjoint process will take a continuous record and window the shots (according to an input recording length and sequence of shot delays) and output a discrete dataset. Thus the forward blending operator requires three inputs - the data, the desired recording length, and a record of shot delays. If the blended data is d_b, and the conventional / separated data is d_s, then the system can be described in equation 5.

$$d_b = \Gamma d_s \tag{5}$$

$$\begin{aligned} J(\mathbf{d}_s) &= \|\mathbf{L}'\mathbf{d}_s - \mathbf{m}\| & (6)\\ J(\mathbf{d}_s) &= \|\mathbf{L}'\mathbf{d}_s - \mathbf{L}'\mathbf{\Gamma}'\mathbf{d}_b\| & (7) \end{aligned}$$

The objective functions for conventional and blended demigration are shown in equation 6. This operator Γ is necessary to calculate the data-space residual (actually the model-space residual, in this case), since a recomputed blended dataset must be used for comparison. For shot separation, the output data will be the recovered data produced after demigration, before it is reblended for comparison.

Three styles of data blending are studied, all with an Ocean Bottom Node (OBN) style geometry. These are: purely random time delays, constant (or linear) time delays, and pseudo-linear delays. These delays are linear in both time and space. For the last style, delays are roughly constant, with a 5% jitter added to the source timings. Example datasets for these three encoding functions are shown in Figure 11, Figure 12 and Figure 13, with the conventional data shown in Figure 10. For these upcoming examples 2D data were used with a fixed receiver geometry. This means the right-hand panel in these figures represents a constant receiver gather, whereas the left panel represents a constant source gather.

For the randomly delayed sequence, all secondary/overlapping energy is incoherent in the receiver domain. This is exploited by all of the aforementioned data-space inversion methods. For the pseudo-linear case, some coherency is induced in these receiver gathers, but the randomness is sufficient such that this may stack out. For the linear case there is no difference in coherency between these domains, so these data-space methods will all fail.

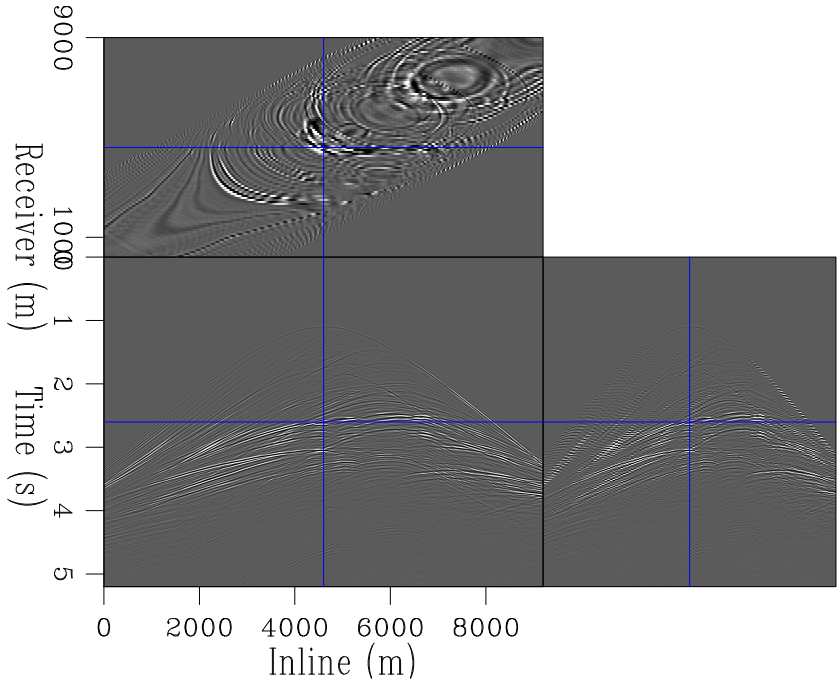

Figure 10: Data acquired over the Marmousi model. [**CR**]

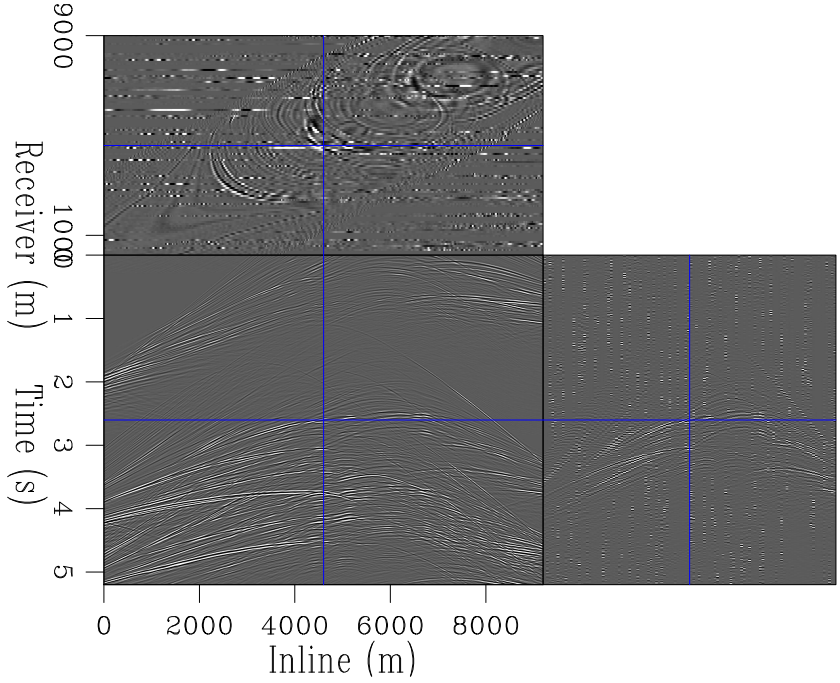

Figure 11: Data acquired over the Marmousi model using a random delay function. [**CR**]

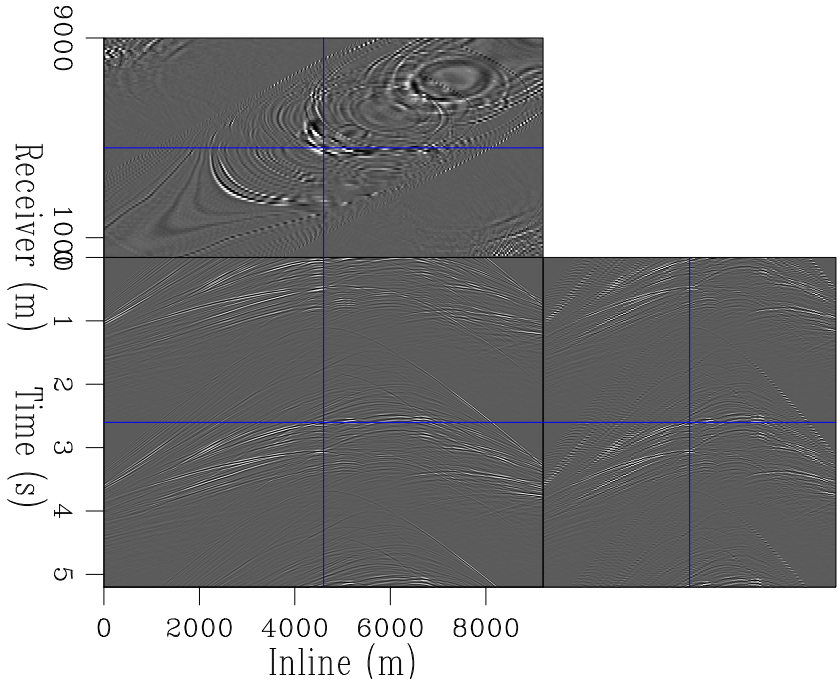

Figure 12: Data acquired over the Marmousi model using a linear delay function. [**CR**]

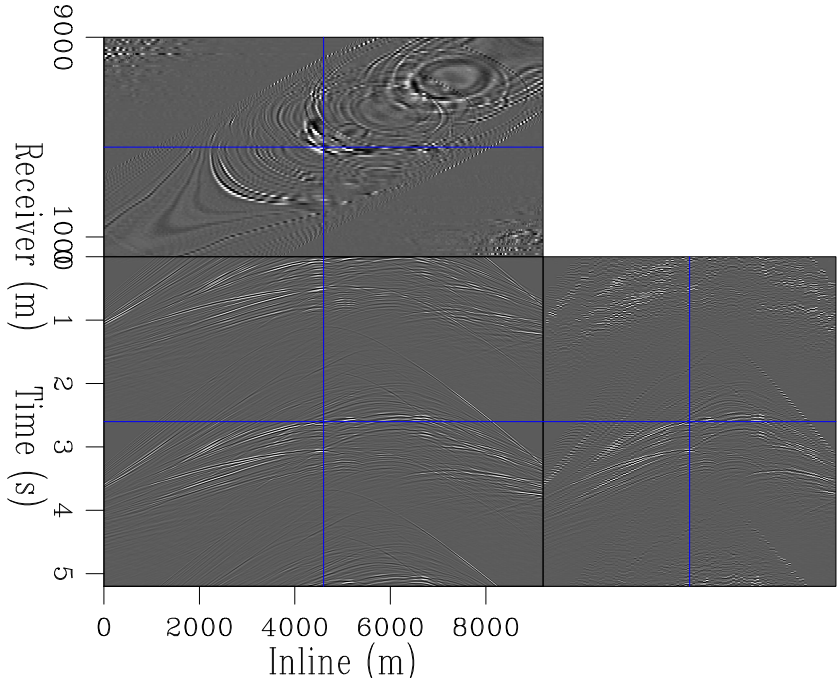

Figure 13: Data acquired over the Marmousi model using a pseudo-linear delay function. [**CR**]

Correct velocity model solution

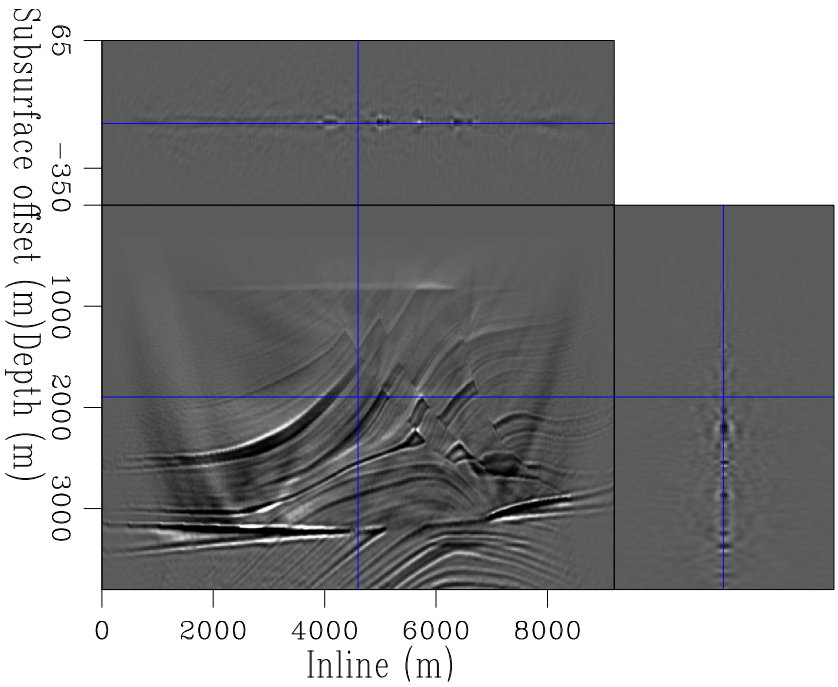

Figure 14: The extended image from migrating Figure 11 (data acquired using a random blending function) [**CR**]

Figure 14, Figure 15 and Figure 16 show the extended images produced from these three datasets using the correct velocity. The differences in blending are manifested in the image space, although the coherency differences are not as pronounced as intuition may suggest. Even the linearly blended data becomes well dispersed in the image space. The artifacts are more coherent, but the focusing characteristics of the primary events, and the differences in contrast, suggest that separation could be possible.

The recovered datasets after adjoint separation can be seen in Figure 17, Figure 18 and Figure 19. Each of the blending schemes have been well separated and the resultant datasets could be used for conventional velocity estimation and imaging. Again, amplitudes at early times and shot offsets are weaker than in reality. This can be improved upon by using the inverse scheme.

It should be noted that there are some fractionally more coherent artifacts in the recovered data from the linear encoding. Nonetheless this methodology separated these linearly delayed data surprisingly easily.

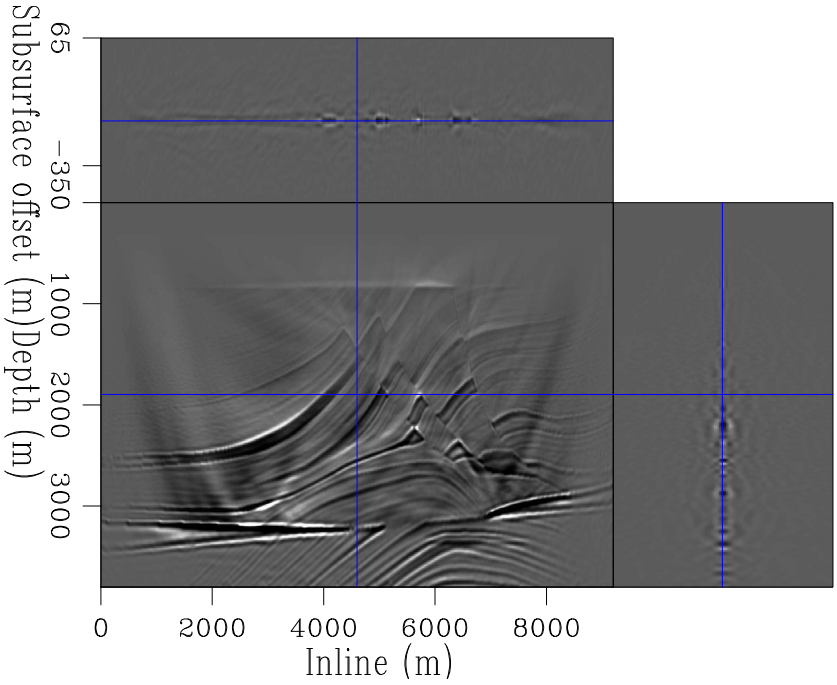

Figure 15: The extended image from migrating Figure 12 (data acquired using constant time delays). [**CR**]

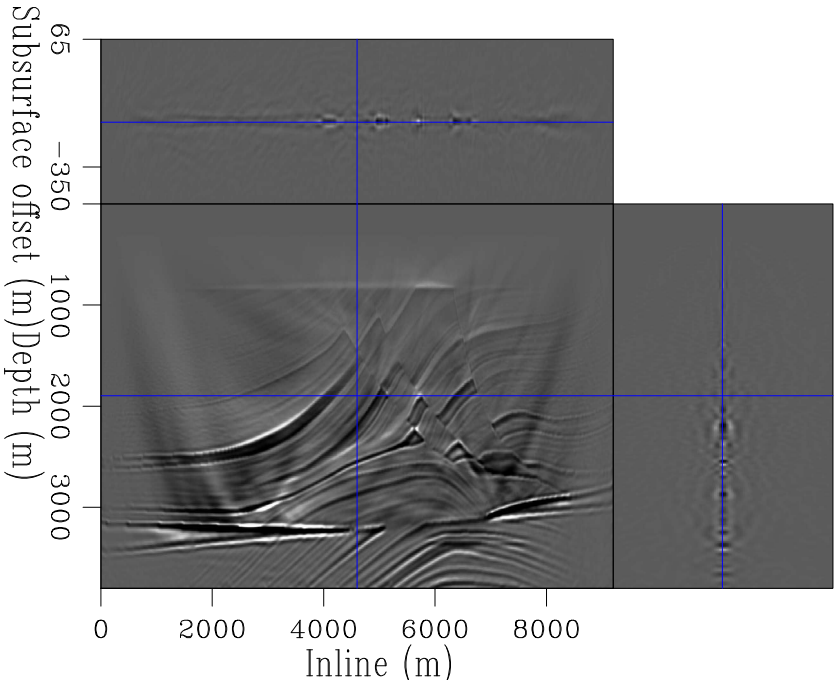

Figure 16: The extended image from migrating Figure 13 (data acquired using pseudo-linear delays). [**CR**]

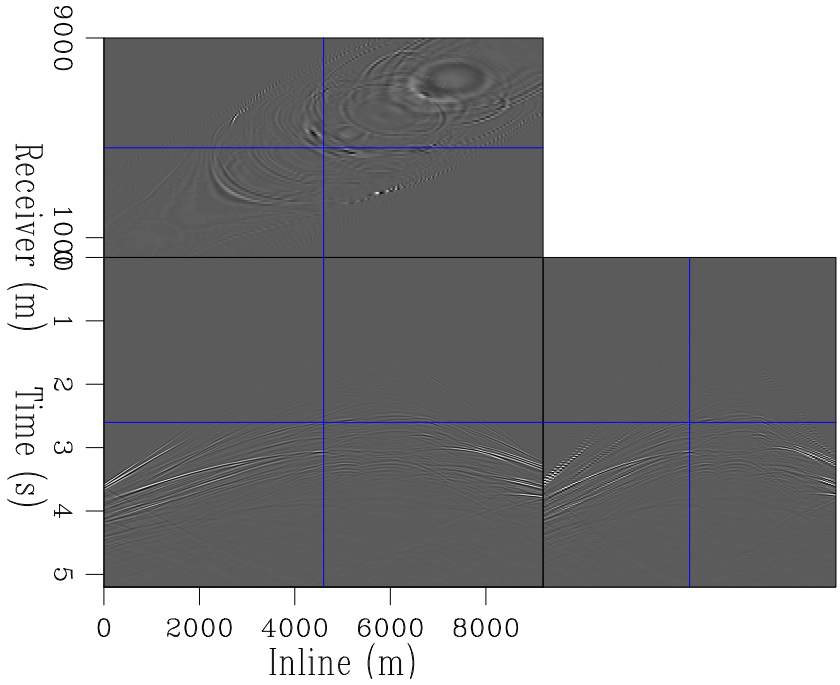

Figure 17: The output dataset after applying adjoint demigration to Figure 14, which was the image created from a randomly delayed dataset. [**CR**]

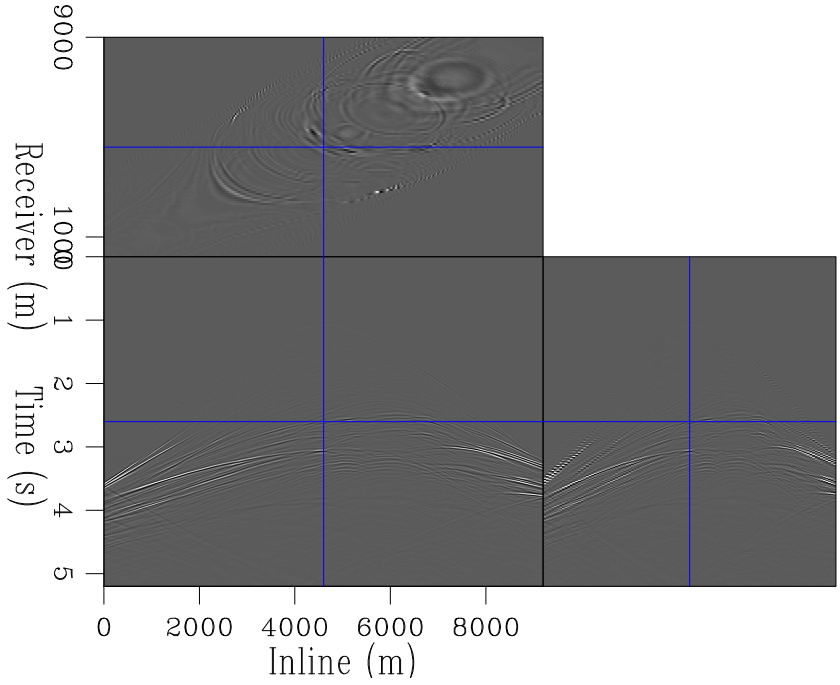

Figure 18: The output dataset after applying adjoint demigration to Figure 15, which was the image created from a linearly delayed dataset. [**CR**]

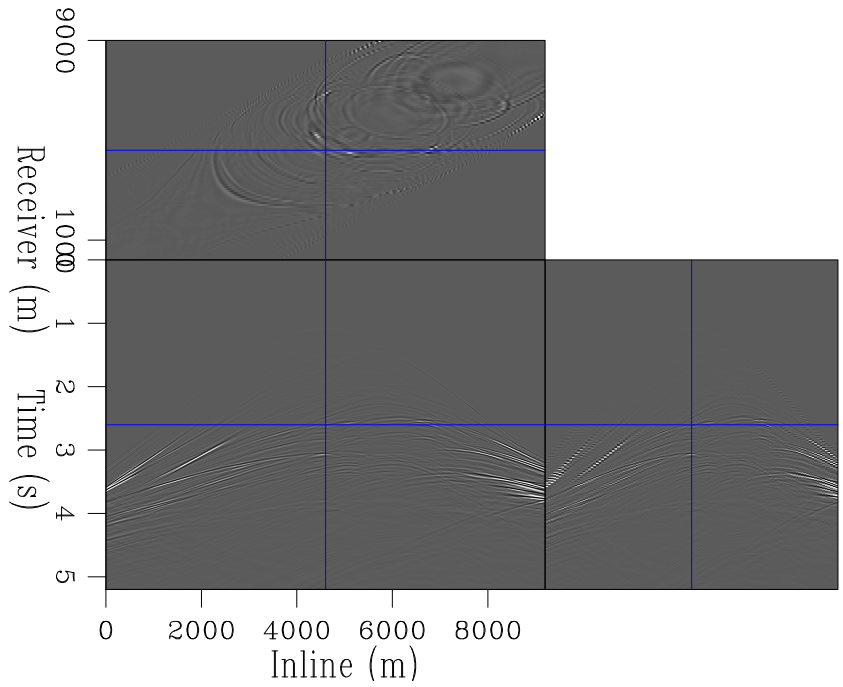

Figure 19: The output dataset after applying adjoint demigration to Figure 16, which was the image created from a pseudo-linearly delayed dataset. [**CR**]

Incorrect velocity model

Separation with an accurate velocity model is a relatively trivial problem. If simultaneous surveys are to be used for exploration then a processing scheme that does not assume strong velocity control is essential. This section will look at these same data, but imaged using a very inaccurate velocity model. The most informative and realistic scenario is pseudo-linear blending, so this will be the acquisition focus from hereon.

Figure 21 shows the result from migrating these data, but using a very rough velocity model. The primary events are now not well focused at zero-subsurface offset, and the focusing contrasts between primary and secondary events is far less. Energy of interest now spans many of the acquired subsurface offsets and distinguishing events from primary and secondary energy is less obvious.

Using data acquired over the Marmousi model gives informative results about the suggested procedure, but to further confidence over this methodology a more difficult example must be used. A section of the SEAM model was windowed, featuring rugose reflectors, continuous reflectors and a steep salt body with carbonate top and sedimentary inclusions. These attributes comprise many of the difficulties of contemporary imaging targets. If this separation method can perform well over these data then much stronger conclusions can be made.

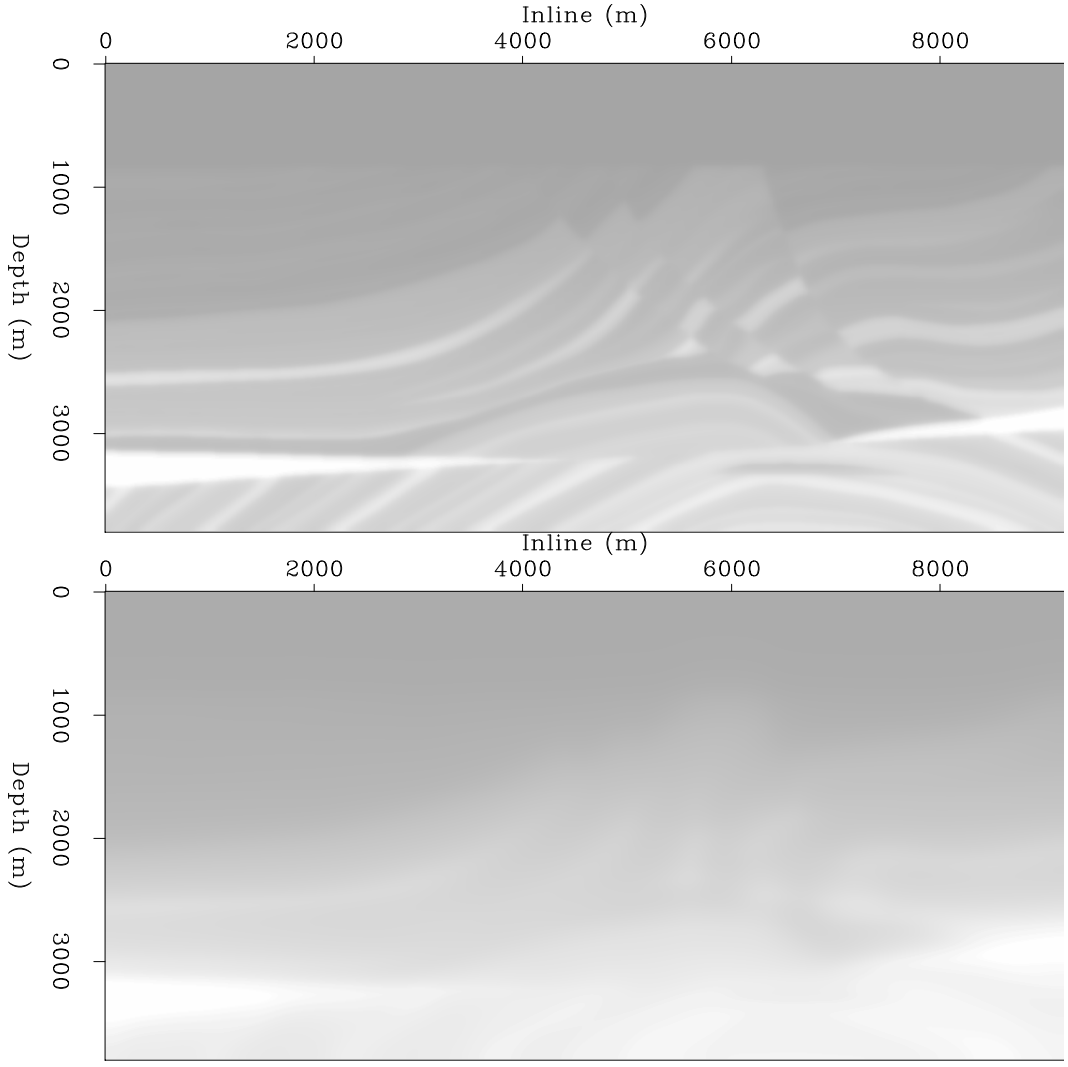

Figure 20: The velocity models used for inverse demigration, correct and incorrect respectively. [**ER**]

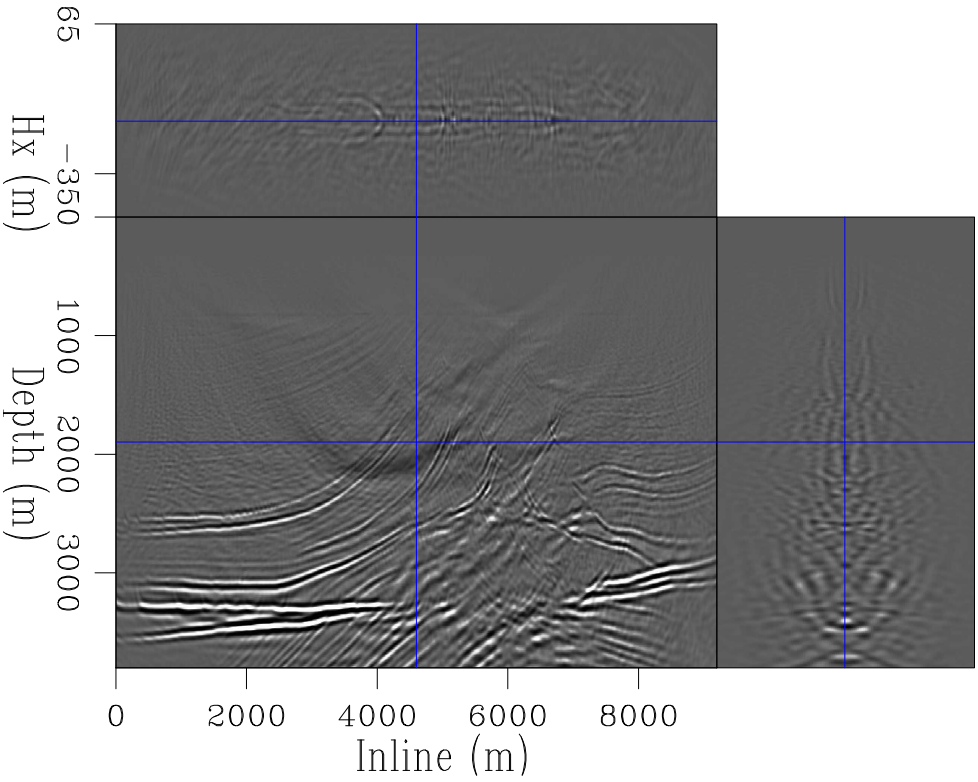

Figure 21: The extended image from migrating Figure 13 (data with constant delays) using a rough velocity model. [**CR**]

SEAM data

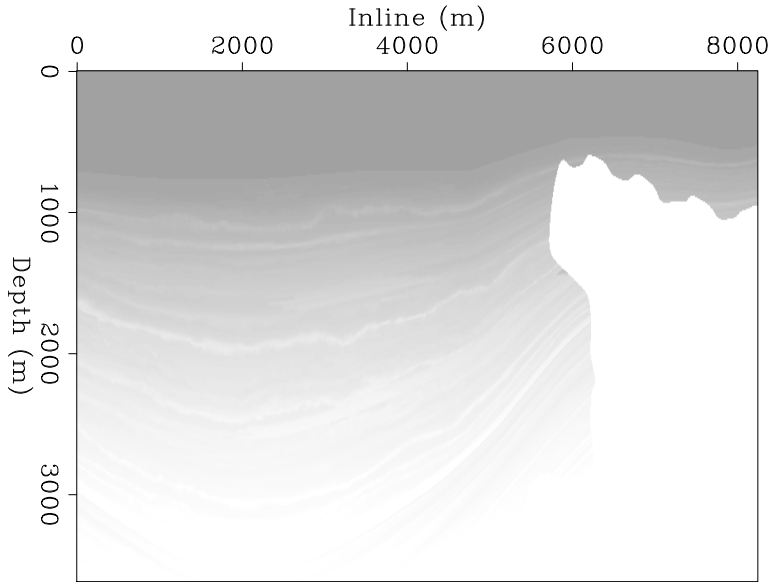

Figure 22: The velocity model windowed from the SEAM model, used for a more realistic separation test. [**ER**]

Data were simulated over the velocity model shown in Figure 22. For this section only a pseudo-linear scheme will be studied, as this is the most realistic encoding that is recorded in the field. One hundred shots were simulated and then combined using a scheme with a blending power of three (similar to three source boats) with constant delays and a 5% timing randomness induced. These data are shown in Figure 24, while the output data after 10 iterations are shown in Figure 25.

These results demonstrate that for a complex model with a variety of impedance contrasts, the separation procedure performs very well. The convergence curve in Figure 26 demonstrates how accurately these data are simulated as a function of iteration number.

AUGMENTATION WITH WEMVA

Extended LSRTM is a very expensive process, and for many geometries and encoding functions this will be more expensive than many of the existing data-space methods. However, there are three circumstances where the suggested inverse demigration process can outperform these algorithms.

The most successful of the data-space methods requires hundreds of 5D FFTs to be performed, so for geometries with sparse, large offsets, this will be a tough undertaking. Furthermore, this method entirely fails with constant time delays, and can induce large artifacts if there is any underlying predictability in the encoding

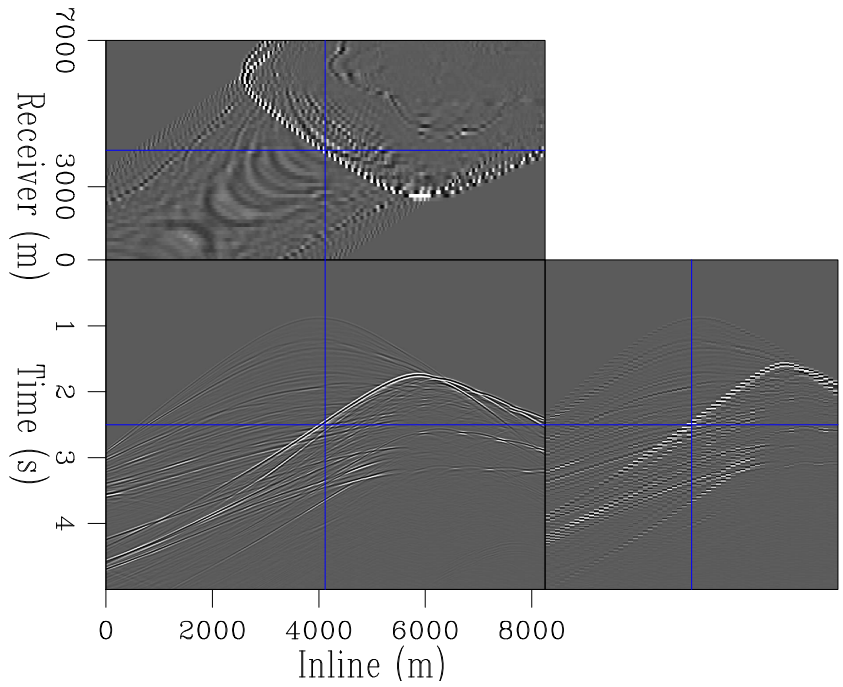

Figure 23: A conventional dataset acquired using the section of the SEAM model. [**CR**]

sequence. So, under these two situations it is likely that extended inverse demigration will outperform a Projection Onto Convez Sets (POCS) type approach.

Thirdly, since extended imaging and modeling are applied, other approaches can take advantage of these spaces. Wave-Equation Migration Velocity Analysis (WEMVA) (Sava et al., 2003) relies on measuring these primary moveouts and using this back-projected information to update the velocity model. With this in mind, image-space shot separation could be easily augmented with WEMVA, where separation is the outer-loop and WEMVA the inner-loop process. This will also provide a positive feedback loop - the more accurate the velocity model has become, the better the separation results are, and fewer subsurface offsets must be collected.

The fact that this separation can be combined with WEMVA makes a powerful argument for the use of such an expensive scheme.

CONCLUSIONS

It is possible to accurately recover input seismic data from the image domain by adapting LSRTM. By using the extended image space, even if imaging was applied using an incorrect velocity model, these data are still recoverable to a high degree of accuracy.

By including a blending operator into this suggested inverse demigration the sys-

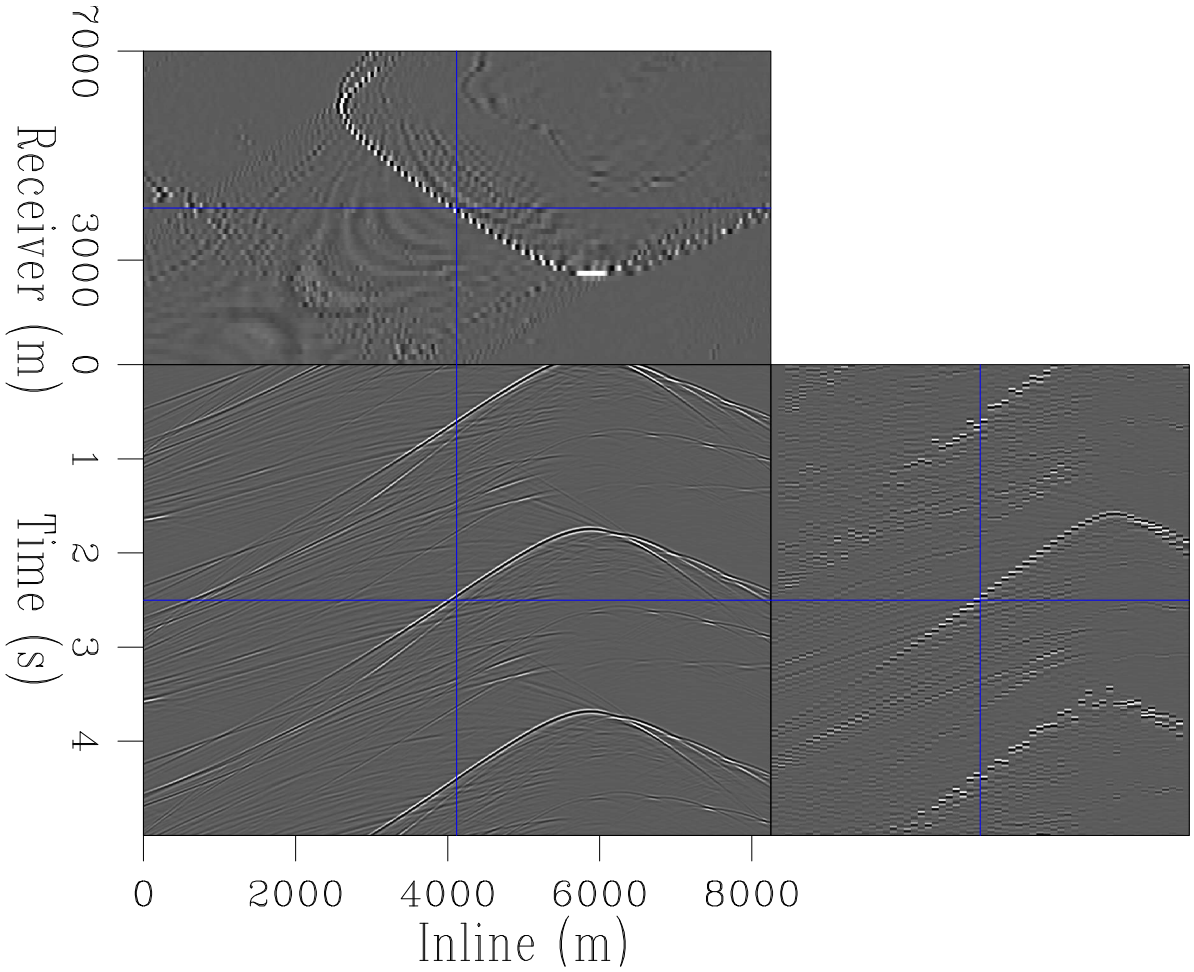

Figure 24: A pseudo-linearly blended dataset acquired using the section of the SEAM model. [**CR**]

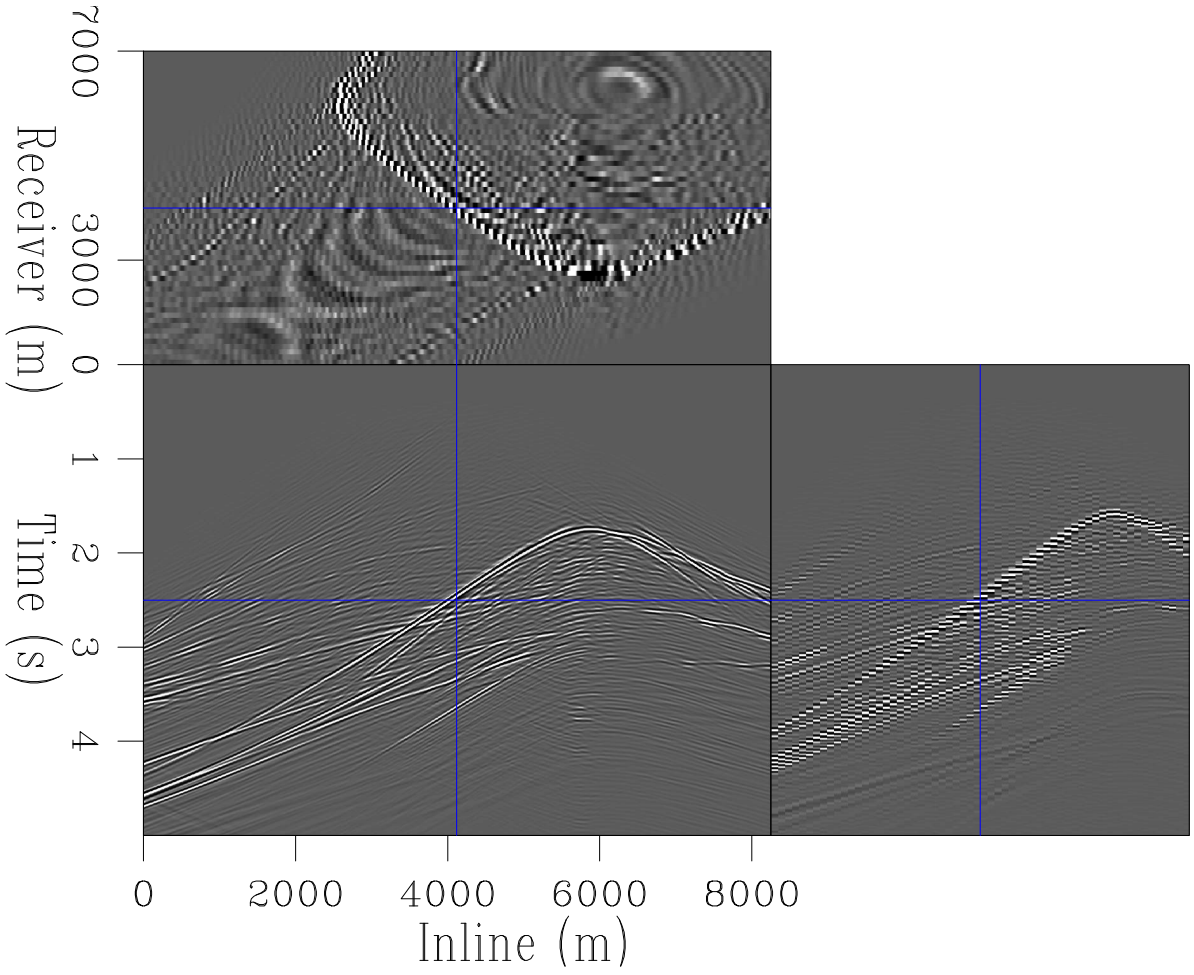

Figure 25: The output separated data after 10 iterations of inverse deimgration using a rough velocity model. [**CR**]

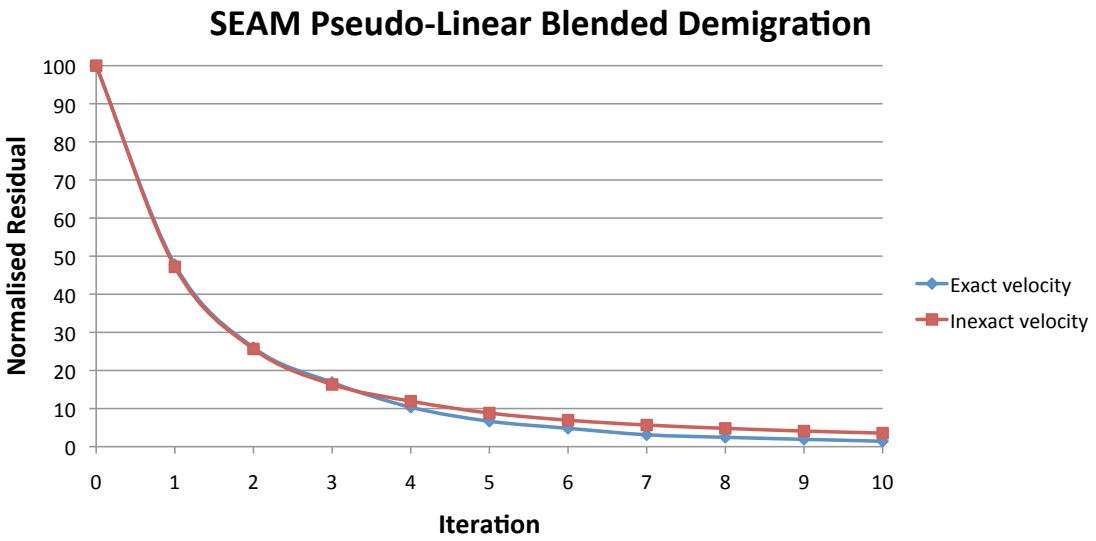

Figure 26: How the separation algorithm performs, for SEAM, as a function of iteration number. [**NR**]

tem can be used to recover an equivalently separated dataset from a continuous, overlapping recording. These separated data are both kinematically accurate and amplitude real, and after re-blending match the input data to within a fraction of a percent. This is true of a synthetic example which features a variety of dips and impedance contrasts.

The fact that extended images have been constructed allows WEMVA to also be applied. Before separation a moveout estimation can be made, and the velocity model updated. This allows both separation and model updating to be applied for almost the same cost.

FUTURE WORK

Tests using field data are currently underway. These are in full 3D for an OBN dataset and the results will be available soon.

ACKNOWLEDGMENTS

The author would like to thank Ray Abma for many insightful discussions about simultaneously acquired data, and all sponsors of the Stanford Exploration Project.

REFERENCES

Abma, R., T. Manning, M. Tanis, J. Yu, and M. Foster, 2010, High quality separation of simultaneous sources by sparse inversion: Presented at the 72nd EAGE Conference & Exhibition.

Abma, R. and J. Yan, 2009, Separating simultaneous sources by inversion: Presented at the 71st EAGE Conference & Exhibition.

Ayeni, G., A. Almomin, D. Nichols, et al., 2011, On the separation of simultaneous-source data by inversion: Soc. Expl. Geophys., Expanded Abstracts, 20–25.

Baysal, E., D. Kosloff, and J. Sherwood, 1983, Reverse time migration: Geophysics, **45**, 1514–1524.

Beasley, C. J., 2008, A new look at marine simultaneous sources: The Leading Edge, **27**.

Berkhout, A., V. D. and G. Blacquiere, 2008, Processing of blended seismic data: SEG Technical Program Expanded Abstracts.

Chauris, H. and M. Benjemaa, 2010, Seismic wave-equation demigration/migration: Geophysics, **75**, S111–S119.

Claerbout, J. F., 1971, Toward a unified theory of reflector mapping: Geophysics, **36**, 467–481.

Dai, W. and J. Schuster, 2009, Least-squares migration of simultaneous sources data with a deblurring filter: SEG Expanded Abstracts, 2990–2993.

Doulgeris, P., A. Mahdad, and G. Blacquiere, 2011, Iterative separation of blended marine data: Discussion on the coherencepass filter, chapter 5, 26–31.

Hampson, G., J. Stefani, and F. Herkenhoff, 2008, Acquisition using simultaneous sources: The Leading Edge, **27**, 918–923.

Herrmann, F. J., Y. A. Erlangga, and T. T. Lin, 2009, Compressive simultaneous full-waveform simulation: Geophysics, **74**, A35–A40.

Leader, C. and B. Biondi, 2014, Image space separation of linearly blended data: SEP-155, **155**.

Moore, I., B. Dragoset, T. Ommundsen, D. Wilson, D. Eke, C. Ward, et al., 2008, Simultaneous source separation using dithered sources: Presented at the 2008 SEG Annual Meeting.

Sava, P., B. Biondi, et al., 2003, Wave-equation migration velocity analysis by inversion of differential image perturbations: 73rd Ann. Internat. Mtg Soc. of Expl. Geophys., submitted.

Sava, P. and A. Guitton, 2005, Multiple attenuation in the image space: Geophysics, **70**, V10–V20.

Sava, P. and I. Vasconcelos, 2011, Extended imaging conditions for wave-equation migration: Geophysical Prospecting, **59**, 35–55.

Tang, Y. and B. Biondi, 2009, Least square migration/inversion of blended data: SEG Expanded Abstracts, **28**, 2859–2863.

Verwest, B. and D. Lin, 2007, Modelling the impact of wide-azimuth acquisition on subsalt imaging: Geophysics, **72**, 241–250.

Zhang, Y. and L. Duan, 2013, Seismic data processing including predicting multiples using a reverse time demigration. (US Patent App. 13/860,567).